NASA/TM—2005-213834 AIAA–2005–3988

System-Level Design of a Shape Memory Alloy Actuator for Active Clearance Control in the High-Pressure Turbine

Jonathan A. DeCastro
QSS Group, Inc., Cleveland, Ohio

Kevin J. Melcher and Ronald D. Noebe
Glenn Research Center, Cleveland, Ohio

July 2005

The NASA STI Program Office . . . in Profile

Since its founding, NASA has been dedicated to the advancement of aeronautics and space science. The NASA Scientific and Technical Information (STI) Program Office plays a key part in helping NASA maintain this important role.

The NASA STI Program Office is operated by Langley Research Center, the Lead Center for NASA's scientific and technical information. The NASA STI Program Office provides access to the NASA STI Database, the largest collection of aeronautical and space science STI in the world. The Program Office is also NASA's institutional mechanism for disseminating the results of its research and development activities. These results are published by NASA in the NASA STI Report Series, which includes the following report types:

- TECHNICAL PUBLICATION. Reports of completed research or a major significant phase of research that present the results of NASA programs and include extensive data or theoretical analysis. Includes compilations of significant scientific and technical data and information deemed to be of continuing reference value. NASA's counterpart of peer-reviewed formal professional papers but has less stringent limitations on manuscript length and extent of graphic presentations.

- TECHNICAL MEMORANDUM. Scientific and technical findings that are preliminary or of specialized interest, e.g., quick release reports, working papers, and bibliographies that contain minimal annotation. Does not contain extensive analysis.

- CONTRACTOR REPORT. Scientific and technical findings by NASA-sponsored contractors and grantees.

- CONFERENCE PUBLICATION. Collected papers from scientific and technical conferences, symposia, seminars, or other meetings sponsored or cosponsored by NASA.

- SPECIAL PUBLICATION. Scientific, technical, or historical information from NASA programs, projects, and missions, often concerned with subjects having substantial public interest.

- TECHNICAL TRANSLATION. English-language translations of foreign scientific and technical material pertinent to NASA's mission.

Specialized services that complement the STI Program Office's diverse offerings include creating custom thesauri, building customized databases, organizing and publishing research results . . . even providing videos.

For more information about the NASA STI Program Office, see the following:

- Access the NASA STI Program Home Page at ***http://www.sti.nasa.gov***

- E-mail your question via the Internet to help@sti.nasa.gov

- Fax your question to the NASA Access Help Desk at 301–621–0134

- Telephone the NASA Access Help Desk at 301–621–0390

- Write to:
  NASA Access Help Desk
  NASA Center for AeroSpace Information
  7121 Standard Drive
  Hanover, MD 21076

NASA/TM—2005-213834 AIAA–2005–3988

System-Level Design of a Shape Memory Alloy Actuator for Active Clearance Control in the High-Pressure Turbine

Jonathan A. DeCastro
QSS Group, Inc., Cleveland, Ohio

Kevin J. Melcher and Ronald D. Noebe
Glenn Research Center, Cleveland, Ohio

Prepared for the
41st Joint Propulsion Conference and Exhibit
cosponsored by the AIAA, ASME, SAE, and ASEE
Tucson, Arizona, July 10–13, 2005

National Aeronautics and
Space Administration

Glenn Research Center

July 2005

This report is a formal draft or working paper, intended to solicit comments and ideas from a technical peer group.

This report contains preliminary findings, subject to revision as analysis proceeds.

Available from

NASA Center for Aerospace Information
7121 Standard Drive
Hanover, MD 21076

National Technical Information Service
5285 Port Royal Road
Springfield, VA 22100

Available electronically at http://gltrs.grc.nasa.gov

System-Level Design of a Shape Memory Alloy Actuator for Active Clearance Control in the High-Pressure Turbine

Jonathan A. DeCastro
QSS Group, Inc.
Cleveland, Ohio 44135

Kevin J. Melcher and Ronald D. Noebe
National Aeronautics and Space Administration
Glenn Research Center
Cleveland, Ohio 44135

This paper describes results of a numerical analysis evaluating the feasibility of high-temperature shape memory alloys (HTSMA) for active clearance control actuation in the high-pressure turbine section of a modern turbofan engine. The prototype actuator concept considered here consists of parallel HTSMA wires attached to the shroud that is located on the exterior of the turbine case. A transient model of an HTSMA actuator was used to evaluate active clearance control at various operating points in a test bed aircraft engine simulation. For the engine under consideration, each actuator must be designed to counteract loads from 380 to 2000 lbf and displace at least 0.033 inches. Design results show that an actuator comprised of 10 wires 2 inches in length is adequate for control at critical engine operating points and still exhibit acceptable failsafe operability and cycle life. A proportional-integral-derivative (PID) controller with integrator windup protection was implemented to control clearance amidst engine transients during a normal mission. Simulation results show that the control system exhibits minimal variability in clearance control performance across the operating envelope. The final actuator design is sufficiently small to fit within the limited space outside the high-pressure turbine case and is shown to consume only small amounts of bleed air to adequately regulate temperature.

Nomenclature

A_{act}	Total HTSMA cross sectional area, $N\pi d^2/4$
A_s, A_f	Austenite start, austenite finish temperature
d	Wire diameter
E	Young's modulus
F_{act}	Actuator force, σA_{act}
F_{pre}	Spring preload force
F_{shd}	Shroud force
g	Clearance gap
g_{cold}	Cold clearance
g_{des}	Desired clearance
I	Control current
K	Spring constant
L	Wire length
M_s, M_f	Martensite start, martensite finish temperature
N	Number of wires
N_{act}	Number of actuators
Q_{bleed}	Fan bleed air flow rate
T	Wire temperature
T_∞	Ambient temperature
x	Spatial variable
x_{act}	Actuator displacement, εL
x_d	high-pressure turbine (HPT) component deformation
ε	Material strain

ε_{max} Maximum material strain
σ Total tensile stress
σ_S^{cr}, σ_f^{cr} Start critical stress, finish critical stress
ξ, ξ_S, ξ_T Total martensite fraction, stress-induced martensite fraction, temperature-induced martensite fraction

I. Introduction

Active clearance control systems in the high-pressure turbine (HPT) section of commercial aircraft engines are used to close the gap that exists between the turbine blades and shroud, hence minimizing leakage flows past the blade. A salient benefit of reducing leakage flow is to minimize specific fuel consumption (SFC) during cruise, potentially saving the airline industry millions of dollars every year and lowering environmentally-harmful NO_x emissions (ref. 1). Another potential benefit is to reduce exhaust gas temperature (EGT) overshoot during takeoff, a critical factor in extending the on-wing life of hot-section components and improving time between engine overhauls (ref. 2).

Clearance control systems used in modern engines rely on matching thermal expansions of turbine components by actively cooling the outer case with available bleed air. Mechanical growth changes of the rotor are experienced as engine thrust demand varies during the course of a mission, but cannot be mitigated because of the limited bandwidth of thermal systems. Hence, modern engines are unable to fully reap benefits of active clearance control. A more effective control system would exploit high-accuracy/high-bandwidth clearance sensing and actuation systems capable of achieving tight clearances over all operating transients. Innovations in high-temperature blade tip proximity probes, like the 25 MHz microwave probe disclosed in Geisheimer et al. (ref. 3), open the door for accurate data-based closed loop control, as opposed to the model-based methods currently used. To bring this technology to maturity, accurate models and simulation of turbine tip clearance (ref. 1) and experimental evaluation of clearance control systems are necessary (ref. 4). Recent advances in the reliability, durability, availability, and energy capability of shape memory alloys make them particularly attractive for actuation (ref. 5).

Shape memory alloys (SMAs) have emerged in several areas, including robotics, control of space-borne structures, and control of helicopter rotor blades (refs. 6 to 9). Some SMA materials, such as Nitinol, allow for strain capabilities up to 6 percent and stress output of 500 MPa (ref. 5). Compared with other smart materials, this represents more than an order-of-magnitude higher energy output per unit density of material. The design can therefore offer a small, lightweight package without needing motion amplifiers that can cause efficiency losses and introduce an additional failure mode. SMA materials may be easily and inexpensively formed into geometries that are structurally viable, with nearly as much freedom in manufacturability as conventional metals. Unlike other smart actuators, SMAs respond to thermal stimuli, so actuator designs can employ modulated hot and cool secondary air to excite the actuator, preventing potentially costly modifications to onboard power systems (ref. 10). Although the material does exhibit a high amount of hysteresis, several authors have achieved position control without significant tracking error using well-established methods, including proportional-integral-derivative (PID) control laws (ref. 11). Certainly, moderate rate requirements of active clearance control are within reach by SMAs, therefore these materials are an excellent match for this application.

The goal of the present work is to demonstrate the feasibility of the proposed SMA prototype actuator through a system-level design and transient simulation in a candidate aircraft engine. The long-term intent is to fabricate and evaluate the prototype in an HPT tip clearance test rig at the NASA Glenn Research Center (ref. 4). The SMA concept design used in the system-level evaluation is discussed first. Here, details of a newly-developed high-temperature SMA material, the relevant parameters involved, and procedures used to design the actuator are outlined. Presented next is the foundation of the analytical feasibility study, the SMA actuator model. In this section, constitutive equations, hysteresis model, and thermal model of the actuator are described. Integration with a test bed simulation of a large aircraft engine is also discussed. Numerical simulation results are then discussed which includes results of parametric trade studies and feasibility evaluation. In this section, the controller used to regulate tip clearance is described. The paper concludes with a summary of the findings and recommended future work.

II. Actuator Concept Definition and Development

Active clearance control is necessary to prevent large clearance variances from occurring throughout normal flight missions. Active control systems must maintain tighter clearances than can be realized at present, so it is essential for the actuator to match the rate and magnitude over the operating envelope in order to avoid detrimental blade incursions (rubs). In modern engines, clearance is initially roughly 0.1 inches at the low-power conditions, then reduces to a fraction of that value at high-power. Because fastest clearance rates-of-change occur during takeoff, the actuator's rate criteria must be based on that event. Approximate HPT conditions for a large gas turbine

TABLE 1.—APPROXIMATE HPT CONDITIONS IN A HIGH-BYPASS GAS TURBINE ENGINE

Specification	Value	
Max. clearance	~0.1	in
Max. clearance rate-of-change	~0.01	in/sec
Max. force from shroud pressure differential	2200	lbf
Number of shroud segments	20	---
Shroud surface area	12	in^2
Number of clearance probe sensors	3	---
Headroom between case and shroud	2	in
Max. air temperature inside case	> 1300	°F
Max. air temperature outside case	600	°F

engine are given in table 1, adapted from DeCastro and Melcher (ref. 12). Pressure differentials across the HPT shroud arise from the fact that compressor discharge air is blown across the outside of the ring to keep the metal cool relative to the hot interior combustor exhaust gas. As a result, the shroud segments that make up the ring are subject to highest forces at maximum power. The compressor discharge air that is used for cooling is at a relatively high temperature that is well above survivability temperatures of any commercial-grade smart material actuator, so it is necessary for the actuator to be located in the thermally isolated environment on the exterior of the case.

The actuation scheme chosen for the active tip clearance control project will independently actuate each shroud segment relative to the blade tips. Clearance is expected to be measured using three or more high-bandwidth proximity probes, in conjunction with estimation laws to determine the clearance at other points around the circumference. Independent actuation allows for automatic adaptation to asymmetric factors such as non-concentricity, ovalization, and flight-maneuver loads, and hence is desirable in maintaining very small clearances (ref. 12). In this work, the target tip clearance is 0.005 inches at all operating points throughout the flight envelope.

SMA Material Selection

Actuators considered for active turbine tip clearance control devices should be able to withstand extreme temperatures at the high-pressure turbine case as well as meet control system operational requirements. SMA materials currently being developed at the NASA Glenn Research Center, offering high robustness at elevated temperatures, are therefore ideal candidates for the present application. The high-temperature shape memory alloy (HTSMA) composition under consideration is nickel-platinum-titanium ($Ni_{30}Pt_{20}Ti_{50}$), which exhibits oxidation rates about half that of typical nickel-titanium (NiTi) SMA materials that are widely used (ref. 13). This allows for indefinite operation at temperatures up to 500 °C (930 °F). Moreover, the transformation temperatures for this material are much higher than typical NiTi alloys, requiring less cooling air to maintain temperature just below these levels. It is also promising that hysteresis of the HTSMA is narrower than the NiTi alloy, a desirable characteristic for closed loop control. For illustration, a typical SMA hysteresis loop is given in figure 1.

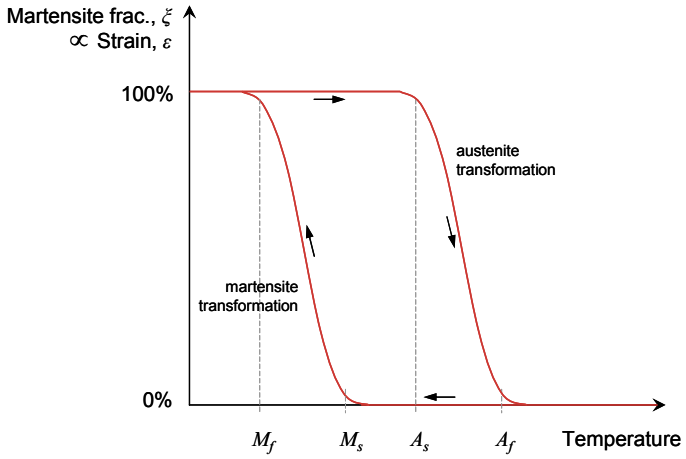

Figure 1.—Major loop hysteresis of a typical SMA.

TABLE 2.—PHYSICAL PROPERTIES OF $NI_{30}PT_{20}TI_{50}$

Parameter		Value		Parameter		Value	
Martensite start temperature	M_s	510	°F	A_s stress influence coefficient	C_{As}	1.78	ksi/°F
Martensite finish temperature	M_f	463	°F	A_f stress influence coefficient	C_{Af}	0.83	ksi/°F
Austenite start temperature	A_s	505	°F	Elastic modulus of martensite	E_M	7000	ksi
Austenite finish temperature	A_f	527	°F	Elastic modulus of austenite	E_A	8500	ksi
Start critical stress	σ_s^{cr}	33.4	ksi	Max. recoverable strain	ε_L	3.3	%
Finish critical stress	σ_f^{cr}	128.6	ksi	Heat capacity	c_v	5.44e6	$J/m^3/K$
M_s stress influence coefficient	C_{Ms}	0.83	ksi/°F	Density	ρ	0.0975	lb/in^3
M_f stress influence coefficient	C_{Mf}	1.44	ksi/°F	Resistivity	ρ_e	4.02e-5	Ω-in

Material properties for the HTSMA are given in table 2. The relevance of these parameters to the actuator model will be discussed in section III. Critical stresses and maximum recoverable strain ε_L were obtained from room temperature stress-strain tests. Transformation temperatures and stress influence coefficients were determined by strain-temperature measurements performed under various constant loads. Young's moduli were found by an impulse frequency excitation technique. Further details can be found in reference 13.

Actuator Concept

Figure 2 shows a schematic diagram of the actuator concept in the present study. SMA material is most readily available in wire form, so fabrication costs of a prototype actuator are lessened if wire-based actuator designs are considered. Additionally, having multiple wires improves failure redundancy and allows thermal effects to propagate through the material at a faster rate. The actuator consists of a series of HTSMA wires attached to a fixed point on the outside of the turbine case at one end and the actuation rod at the other. The rod is attached to a single shroud segment that is free to move in the radial direction in order to open or close the clearance gap. Compressor discharge air is always at a higher pressure than the gas path air on the inside, so the net force always acts to compress or buckle the wires. A spring is therefore installed in parallel with the wires and pre-loaded against a mechanical stop to keep the wires in tension and provide clearance restoration in the event of mechanical failures.

The actuator operates as follows. When the wire temperature is low, the material exists in the martensite phase, at which point strain is greatest and the shroud is positioned furthest from the blades. When heated past a certain temperature, the material transitions to austenite, causing the wires to shorten in length and move the shroud inward toward the blades. The clearance gap $g(t)$ is defined as

$$g(t) = x_{act}(t) - x_d(t) + g_{cold} \tag{1}$$

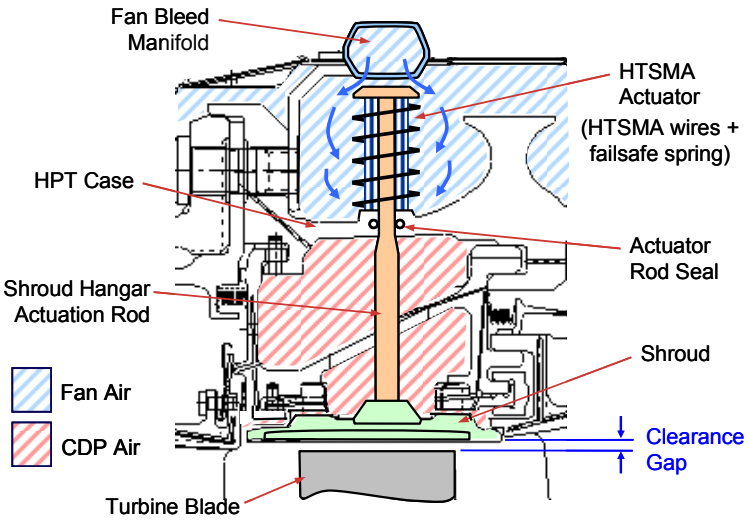

Figure 2.—HTSMA active clearance control actuator concept.

where g_{cold} is the initial (or cold) clearance determined from design, $x_d(t)$ represents the combined inward (toward the blades) deformation of HPT subcomponents relative to the cold clearance, and $x_{act}(t)$ is the actuator deflection.

The abundance of energetic secondary air in aircraft engines allows utilization of this air to cool the material to below the material's transition temperatures. In this setup, secondary air diverted from the engine's fan will be used to impart cooling on the wires. Spacing between wires must be kept relatively large in order to promote rapid, uniform heat transfer across the entire actuator so that each wire reaches transition at similar time instants.

For this study, resistive heating via current modulation was chosen to regulate HTSMA wire temperature. For a prototype proof-of-concept ACC system, this method is preferred due to ease of implementation and fast heating time (ref. 10). Installation of power amplifiers has always been a practical shortcoming for implementing smart materials in aircraft engines, so it is envisaged to actively cool the wires in future builds by modulating fan air, while utilizing the high-temperature ambient surroundings for passive heating. Unfortunately, transition temperatures of the present HTSMA material are higher than the environmental temperature at some critical points in the operating envelope, so the feasibility of using active cooling was not evaluated here. It should be pointed out that, because the likelihood of blade incursions is greatest during low-to-high power transitions, such as takeoff, cooling times are of larger concern than heating times. This signifies that resistive heating is adequate for assessing clearance control capabilities for either actuation mode. To reasonably assess the efficacy of active cooling methodologies, a subset of viable HTSMA materials with various transition temperatures must be evaluated. However, material composition is inherently tied with physical properties, so a more expansive trade study is required for a full evaluation to be possible.

III. HTSMA Actuator Model

To evaluate the active clearance control actuator and demonstrate viable control strategies, a transient 1–D thermomechanical model is coupled with a commercial engine simulation (CES) test bed representative of a large aircraft engine. A block diagram of the simulation setup is shown in figure 3. The actuator model consists of three parts: an SMA quasi-static constitutive equation, hysteresis model, and heat transfer model. The HTSMA hysteresis model is not presented here; however, a detailed exposition of the model developed for this study is given in reference 13. This model proposes an algorithm akin to the generalized Preisach method to represent minor hysteresis loops, and is critical for closed-loop control evaluation (ref. 14).

Quasi-Static SMA Model

Several SMA thermomechanical evolution models have been developed that are derived either from first-principles or phenomenology. Of the several models considered, none have broader applicability than the Brinson model because of the distinction made between stress- and temperature-induced martensite variants (ref. 15). This is especially important for predicting stress-related effects at low temperature (ref. 16). The region in which martensite transitions between variants is labeled **S** in the stress-temperature plot from figure 4(a). As stress is applied through region **S**, it transitions from temperature-induced martensite to stress-induced martensite, causing large strains to develop. Hence, the energy output of the wire increases with applied stress. As shown in figure 4(b), restoration of

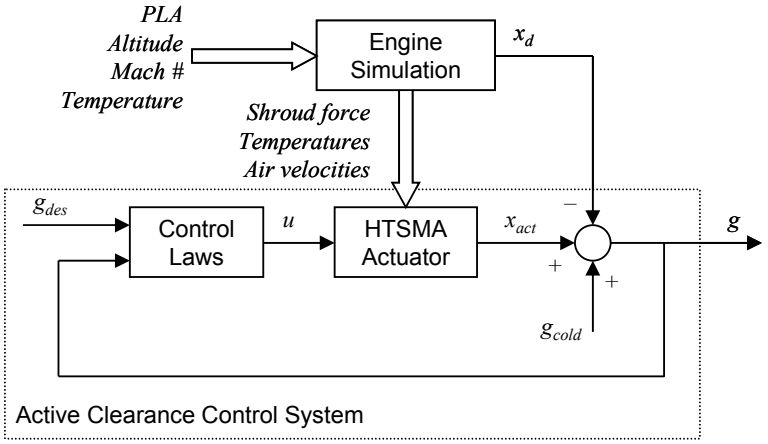

Figure 3.—Block diagram of active clearance control architecture.

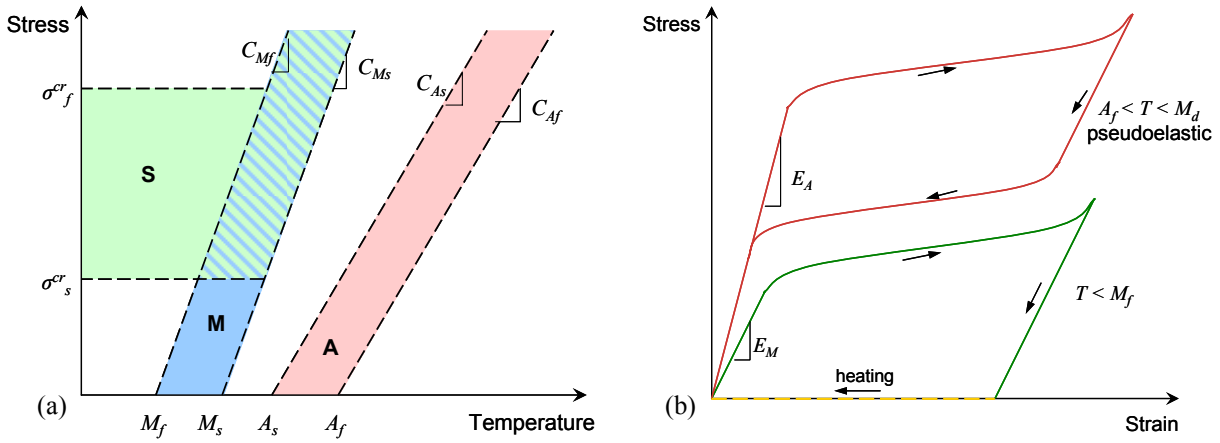

Figure 4.—(a) Transition stress-temperature behavior and (b) isothermal stress-strain characteristics of a typical SMA.

the strain cannot be achieved unless the material is heated to austenite, a process commonly referred to as the *shape memory effect*. Regions where austenite transformation occurs, denoted **A** in figure 4(a), and where martensite occurs, denoted **M**, have an approximate linear dependence with applied stress. Because regions **A** and **M** are not identical, a hysteresis loop forms when temperature and stress are varied. Stress variations at temperatures above A_f, but below the martensite deformation temperature M_d, can result in complete strain recovery, known as the *pseudoelastic* effect as depicted in figure 4(b).

The Brinson model describes the quasistatic thermomechanical evolution by first separating total martensite fraction ξ into a stress-induced component ξ_S, and temperature-induced component ξ_T

$$\xi = \xi_S + \xi_T \tag{2}$$

The constitutive equation relating the two martensite states and the strain ε, stress σ, and temperature T is as follows:

$$\sigma - \sigma_0 = E(\xi)\varepsilon - E(\xi_0)\varepsilon_0 + \Omega(\xi)\xi_S - \Omega(\xi_0)\xi_{S0} + \Theta(T - T_0) \tag{3}$$

where the subscript 0 denotes the initial states, E is the modulus of elasticity, Ω is the phase transformation coefficient, and Θ is the coefficient of thermal expansion (CTE). In this study, CTE is assumed to be negligible.

As shown in figure 4(a), the boundaries of transformation region **S** are defined by the starting critical stress σ_s^{cr} and the finish critical stress σ_f^{cr}. Transformation region **A** is bounded by the austenite start and austenite finish temperatures (A_s and A_f, respectively) which are linearly dependent on stress. The slopes of each line are defined by the respective stress influence coefficients C_{As} and C_{Af}, which are defined in table 2. Likewise, transformation region **M** in figure 4(a) is bounded by martensite start and finish temperatures (M_s and M_f, respectively), with slopes defined by C_{Ms} and C_{Mf}. Evolution of martensite fraction between these bounds is approximated with a cosine relationship (ref. 17). The hysteresis model relating temperature and martensite fraction, not described here, incorporates a minor-loop algorithm that computes the martensite fraction trajectory based on current temperature and a limited horizon of the trajectory history (ref. 13).

Heating and Cooling of Actuator Wires

Heat transfer in the space outside the HPT case is largely driven by convection, as fan discharge air will be used to cool the wires below transition. Conduction may also be significant with designs where the form factor (length-to-diameter) is small. One-dimensional heat conduction is described by:

$$\frac{c_v}{k}\frac{\partial T(x,t)}{\partial t} = \frac{\partial^2 T(x,t)}{\partial x^2} - \frac{4h(t)}{kd}\left[T(x,t) - T_\infty(t)\right] + \frac{16\rho_e}{\pi^2 k d^4} I(t)^2 \tag{4}$$

where c_v is the heat capacity, k is the thermal conductivity, d is the wire diameter, ρ_e is the electrical resistivity, and $I(t)$ is the control current. The ambient temperature $T_\infty(t)$ is obtained from the CES test bed. The convection coefficient $h(t)$ is defined as follows for a cylinder in a uniform, forced cross-flow (ref. 18):

$$h(t) = \frac{k_{air}}{d}\left\{0.3 + 0.62\,\mathrm{Re}(t)^{1/2}\,\mathrm{Pr}^{1/3}\left[1+\left(\frac{0.4}{\mathrm{Pr}}\right)^{2/3}\right]^{-1/4}\left[1+\left(\frac{\mathrm{Re}(t)}{28.2\times10^4}\right)^{5/8}\right]^{4/5}\right\} \tag{5}$$

Here k_{air} is the thermal conductivity for air, Re(t) is the Reynolds number, a function of the time-varying air velocity, and Pr is the Prandtl number. Temperatures at the wire boundaries $T(0,t)$ and $T(L,t)$ are assumed to be equal to the case metal temperature $T_c(t)$, known from the CES. When used in the hysteresis model, wire temperature is taken simply as the average of the temperature distribution along the wire within 5 °C of the temperature at mid-span. An effective wire length is conservatively computed as the distance over which the temperature distribution is within 5 °C of the mid-span temperature.

CES Test Bed Simulation

A high-fidelity simulation of a high-bypass turbofan engine is used as the test bed for the HTSMA actuator. The CES features a detailed model of the HPT section, allowing the actuator model to be integrated with very few approximations. In the CES, one can extract gas path and secondary air temperatures, pressures, and flow rates as well as temperatures and deflections of the various HPT sub-components. As shown in figure 3, simulation inputs are the following environmental variables: altitude, Mach number, ambient temperature, and power lever angle (PLA).

Shroud force is related to the pressure differential acting on the inner and outer surfaces of the shroud ring, estimated as

$$F_{shd}(t) = A_{shd}\left[0.8P_3(t) - P_4(t)\right] \tag{6}$$

where the inner and outer surface area A_{shd} is 12 in^2, and where subscripts 3 and 4 represent the compressor discharge air (station number 3) and HPT inlet air (station number 4), respectively.

Fan bleed air, used in state-of-the-art (SOA) thermal clearance control via external case cooling, is used here for passive HTSMA actuator cooling. It is assumed that the ducting is modified to force air only at discrete locations around the circumference where each actuator is situated. Cold air flow $Q_{cold}(t)$ across one actuator is

$$Q_{cold}(t) = \frac{Q_{bleed}(t)}{N_{act}} \tag{7}$$

where $Q_{bleed}(t)$ is the total flow diverted from the fan for SOA thermal clearance control and N_{act} is the number of actuators, here equal to 20. Assuming the flow travels mostly in parallel to the wires, velocity can be estimated by using an annular flow path area of 3 in^2. The cool air temperature $T_{bleed}(t)$ is known from the simulation. Leakage of hot compressor air past the actuator plunger rod seal can have a substantial impact on ambient air temperature. The hot air flow $Q_{hot}(t)$ is computed:

$$Q_{hot}(t) = C_v\sqrt{(P_3 - P_{amb})/SG} \tag{8}$$

The flow coefficient C_v is equal to 0.002 ft^3/min $\sqrt{\mathrm{psi}}$ and is an estimate based on leakage experiments conducted on the HPT tip clearance test rig. Ambient pressure P_{amb} is an environmental variable and the specific gravity SG used here is 1.0. Because leakage flow enters the cavity between the plunger rod and actuator wires, hot air flow area is identical to the cold flow area.

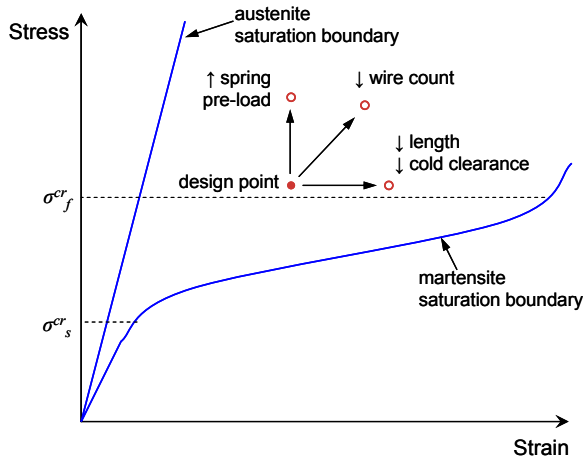

Figure 5.—HTSMA saturation regions and design strategy.

IV. HTSMA Actuation System Design

SMA saturation boundaries identified in figure 5 delineate the operable envelope of the actuator. As actuator design parameters are varied, the influence this has on the location of a given operating point in the stress-strain space is illustrated in the figure. The figure shows that work output of SMAs becomes appreciable at stresses above σ_s^{cr}, therefore the fundamental design objective is to choose actuator parameters that cause all operating points to lie above σ_s^{cr}. The actuator deflection $x_{act}(t)$ is found from equation (1), with $g = g_{des}$, the desired clearance set point, here assumed to be 0.005 inches. Force on the wires is the sum of the spring force and shroud force:

$$F_{act}(t) = F_{pre} + Kx_{act}(t) - F_{shd}(t) \tag{9}$$

It is important to note that preload on the actuator keeps the wires in tension, while the shroud force acts to lessen tension in the wires. From equations (1) and (9), one can infer actuator strain and stress, respectively. $x_d(t)$ is shown in figure 6 for a normal flight mission, as well as the force acting on the shroud, as defined by equation (6). The 'pinch point' designation refers to the point at which clearance reaches a minimum, which approximately coincides with maximum EGT overshoot. From figure 6 and equation (1), it is evident that the actuator must displace the least at low-power operating points (ground idle) and must displace a large amount at high-power points (takeoff pinch

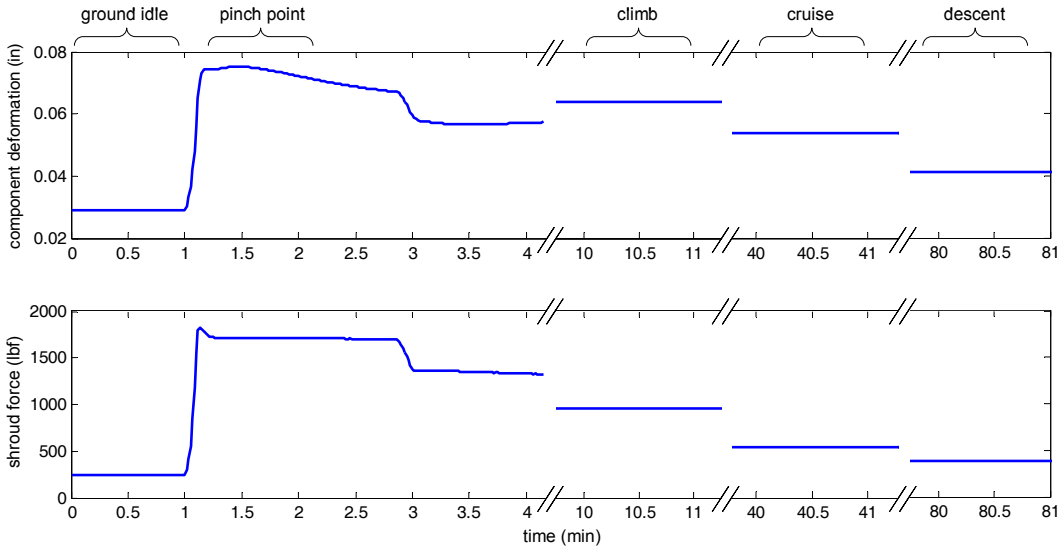

Figure 6.—CES test bed mission profile.

point), thus 'ground idle' and 'takeoff pinch point' are chosen as the two design constraints. Specifically, at ground idle, x_d = 0.028 inches, and at the pinch point, x_d = 0.074 inches, resulting in a net actuator displacement of 0.046 inches. However, since active clearance control is less beneficial at ground idle, that point in the map may be disregarded in an effort to minimize actuator length. Using the descent condition (x_d = 0.041 inches) as the low-power constraint, an actuator displacement of 0.033 inches is achievable. Because EGT overshoot occurs at the pinch point, EGT mitigation should not be affected if clearance is not controlled during ground idle as long as control is established before the pinch point. For the quasi-static design, a map of several steady-state operating points is used to design the actuator, with several points included in the mission profile of figure 6.

Using 'descent' and 'takeoff pinch point' as the two design constraints, it is possible to calculate the necessary physical parameters such that the CES operating points fit tightly within the actuator's stress-strain envelope. Actuator preload force, spring constant, cold clearance bias, and HTSMA cross sectional area are all found by iteratively solving equations (1), (3), and (9) to find an optimum design based on the design strategy illustrated in figure 5.

If wire length and maximum strain are specified, the solution is unique for the remainder of unknown parameters. In effort to maintain high HTSMA cycle life, it is desirable to limit peak strain to within 3.0 percent under all conditions. In order to reduce wire length, a key motivation for an acceptable design, it is evident from figure 5 that the strain requirement must increase. Trade curves in figure 7 show that it is possible to simultaneously obtain wire lengths less than 2 inches and strains less than 3.0 percent by appropriate selection of the remaining four parameters. If higher cycle life is desired, either longer lengths or substantially larger HTSMA areas and preload forces must be used. It should be cautioned that sensitivity to parameter variations becomes extremely high as designs approach the asymptotes at either extreme of each peak strain curve, therefore designs should stay well

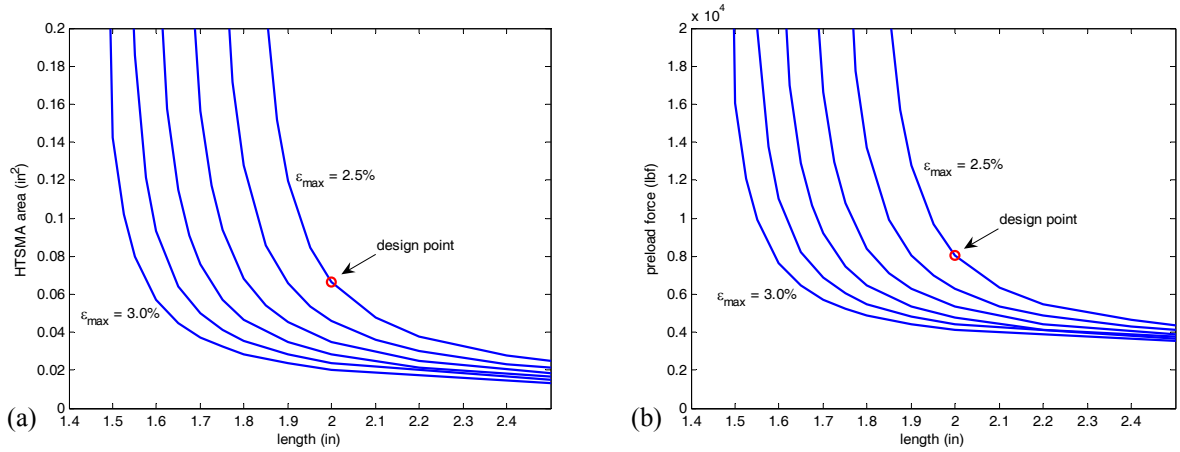

Figure 7.—Effect of wire length and peak strain on selection of: (a) total HTSMA cross sectional area and (b) spring preload.

TABLE 3.—IMPACT OF GROUND IDLE ACCOMMODATION ON ACTUATOR DESIGN FOR HTSMA CROSS SECTIONAL AREA OF 0.0664 IN^2

Design number	Low-Power Op. Point Accommodation	Wire Length (in)	Peak Strain (%)
1	Descent only (Baseline)	2.0	2.50
2	Ground Idle and Descent	2.0	3.32
3	Ground Idle and Descent	2.2	3.08
4	Ground Idle and Descent	2.4	2.88

TABLE 4.—ACTUATOR DESIGN RESULTS

Length (in)	Peak Strain (%)	Mech. Stop Strain (%)	HTSMA Area (in^2)	Cold Clearance (in)	Preload Force (lbf)	Spring Const. (lbf/in)
2.0	2.50	3.00	0.0664	0.090	8040	16080

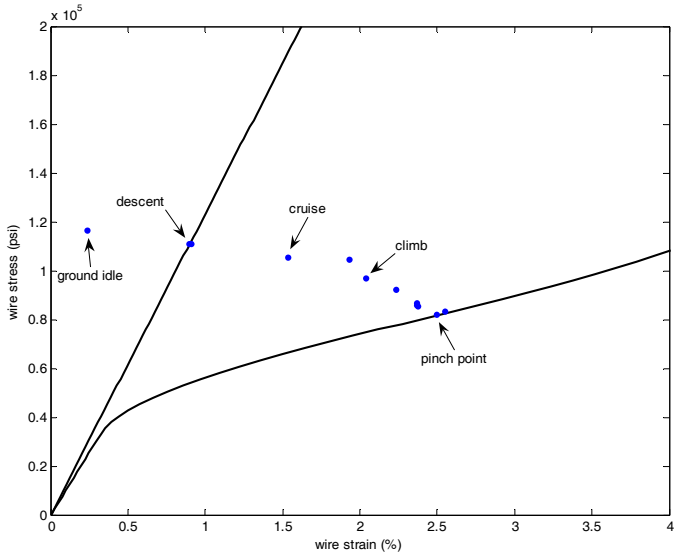

Figure 8.—Engine operating point map with HTSMA saturation regions.

away from those conditions (e.g., by ensuring that area is below 0.1 in^2 and above 0.04 in^2). Table 3 illustrates the impact of accommodating 'ground idle' in addition to 'descent,' confirming that wire length and strain need to be much larger than desired if 'ground idle' is included in the active clearance control objective.

Selecting a wire length of 2.0 inches and a peak strain of 2.5 percent, the operating point map in figure 8 is obtained. Table 4 summarizes the parameters calculated for this design. The spring constant K is chosen to obtain a spring preload deflection of 0.5 inches. The plot confirms that the two-point constraint is satisfactory for the remaining operating points to fit within the stress-strain envelope. If a trial diameter of 0.015 inches is used, the number of wires (N = 376) is excessively large, so larger wire diameters should be sought in order to permit lower counts to be possible. Using the above cross sectional area, the number of wires may be reduced to 10 if each HTSMA wire is increased to 0.092 inches in diameter. A wire diameter such as this may be problematic in meeting the rate requirement, so transient simulations are necessary to verify feasibility. It should be noted that, to preserve failure redundancy, the final design should have a wire count of no less than 10 and is therefore considered to be the design goal. When wires fail, operating points will move to the upper-right portion of the stress-strain space, and thus will likely stay within the saturation envelope.

V. Active Clearance Control Simulation

In this section, the active clearance control system was evaluated in the CES test bed using a transient profile that captures the key elements of a nominal mission. The mission profile scenario used in this section is as shown in figure 6. To evaluate the control system, 10 wires that are each 0.092 inches in diameter are used as a baseline design of the actuator, satisfying the total cross sectional area requirement of 0.0664 in^2. In actual applications, it is possible that re-accel (or re-burst) transients can occur at any time during the mission. Although these transients are more severe in magnitude than takeoff, representative magnitudes of such events are not available, thus re-accel transients were not evaluated here.

Controller

A PID controller with an integrator windup protection scheme was designed for the HTSMA actuation system. This scheme was chosen to avoid large temperature excursions in the phase saturation regions of the material (i.e., at either complete martensite or complete austenite) that may inadvertently cause long delay times in actuator response. The PID control law with back-calculated integrator windup protection (IWP) (ref. 19) is

$$u(t) = K_p\left[e(t) + \int_0^t \left(\frac{e(\tau)}{\tau_i} + \frac{e_1(t)}{K_p\tau_1} + \frac{e_2(t)}{K_p\tau_2}\right)d\tau + \tau_d\frac{d}{dt}e(t)\right] \tag{10}$$

where $u(t)$ is the control variable, $e(t)$ is the error signal, K_p is the proportional gain, and τ_i and τ_d are the integral and derivative time constants, respectively. Here $e_1(t)$ represents how far the actual wire temperature is from material's transition band, $e_2(t)$ is the error between the un-saturated and saturated command current, and τ_1 and τ_2 are the IWP time constants. Since $u(t)$ is directly related to current, no measurement or estimation is necessary to find $e_2(t)$. However, $e_1(t)$ requires either estimation or direct measurement of wire temperature as well as estimation of transition temperature based on actuator force, and hence is a more difficult value to obtain in practice. For the sake of the feasibility study, it will be assumed here that errors between predicted transition bands and actual values are negligible.

The controller objective is to shorten time delays due to hysteresis and to eliminate overshoot. For the physical parameters chosen, Ziegler-Nichols tuning (ref. 20) was used to obtain the following gains: K_p = 106 and τ_i = 7.5 sec, with τ_d set to zero and the IWP parameters τ_1 = 0.01 sec and τ_2 = 0.001 sec. Responses were observed to remain stable and non-oscillatory for all operating transients tested.

Simulation Results

Figure 9 shows an HTSMA active clearance control time trace during the takeoff portion of the mission. The plot shows that the PID control system allows for adequate convergence to the desired 0.005-inch set point. The critical transition point where the integrator transitions from a saturated state to an un-saturated state occurs at 12.4 sec, at which time the controller reduces the current, causing wire temperature to be reduced at a rate of 55 °F/sec to overcome the deadband between A_f and M_s. Before 12 sec, the IWP scheme regulates temperature at slightly above the austenite finish temperature (667 °F), maintaining 100 percent austenite. After 12.4 sec, the PID controller begins to modulate the actuator, causing the system to converge to within 0.001 inches of the set point at 21.8 sec. It should be noted that because EGT overshoot occurs at approximately 25 sec, the above convergence time is marginally acceptable for mitigating this overshoot. These results also confirm that the baseline design is

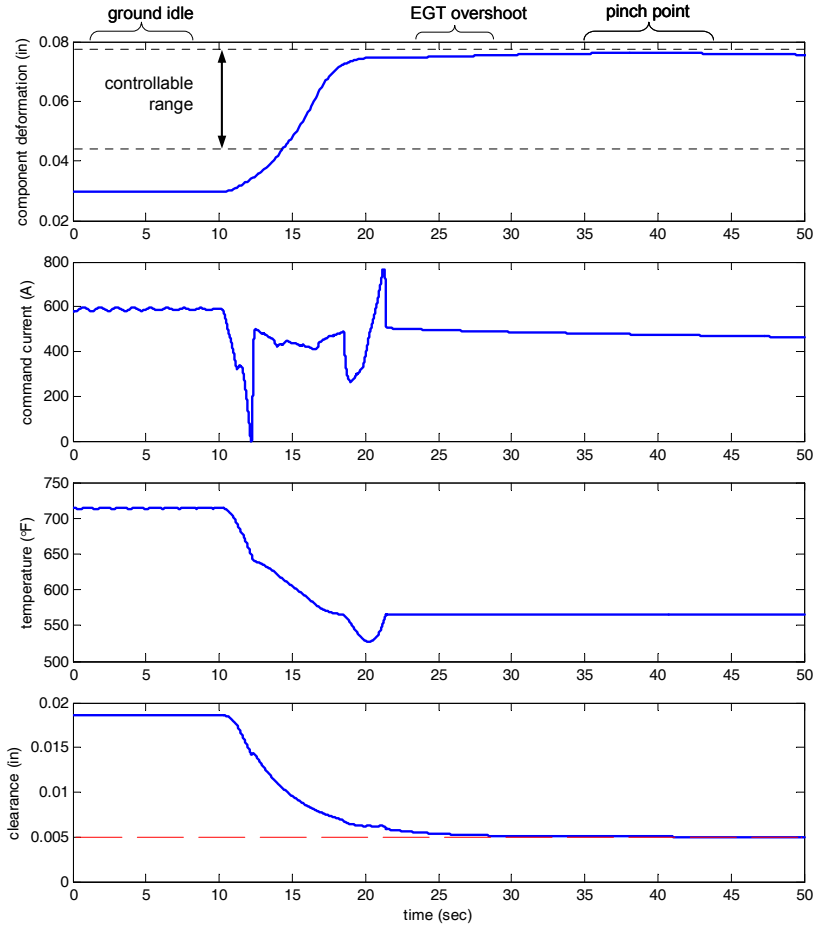

Figure 9.—Active clearance control time trace for takeoff.

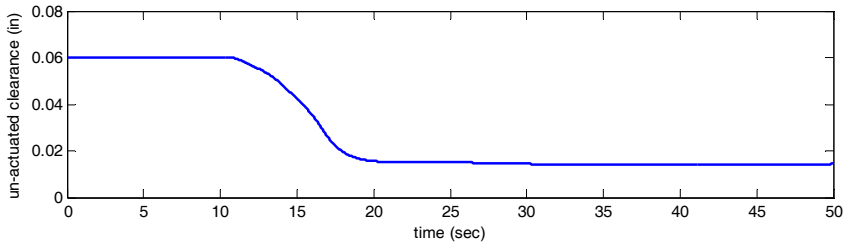

Figure 10.—Takeoff clearance time trace with active clearance control deactivated.

satisfactory in meeting the 0.01 in/sec rate criterion. Additionally, the actuator retains full authority and remains free of oscillation during all portions of the mission other than takeoff. An important observation to make is that the saturated actuator is able to maintain clearance at 0.018 inches at ground idle which, for reference, is substantially less than the 0.060-inch un-actuated ground idle clearance. To illustrate operability upon loss of power and subsequent cooling to 100 percent martensite, the resulting clearance time trace is as shown in figure 10. The pinch point clearance with the control system off is 0.014 inches, which provides for an adequate failsafe against blade rubs.

The effect of incrementally decreasing the amount of fan air used to cool the wires on control system performance for two wire counts (keeping total HTSMA area constant) is shown in table 5. In the table, the controller was re-tuned for each test run according to the Ziegler-Nichols method. After performing the simulation run, minimum clearance, the time at which clearance converges to within 0.001 inches of the set point, and A_f holding current were recorded. From the table, a wire count of 10 yields marginally acceptable performance at air flow bleeds that are 100 and 20 percent of SOA, but convergence time and minimum clearance begin to degrade with bleeds of 5 percent and lower. Because response times improve with surface area, higher wire counts are commensurate with faster response times. With a wire count of 30, acceptable results are obtained at 100, 20, and 5 percent SOA bleeds, but undesirable performance occurs at 1 percent bleed. From another perspective, an actuator with wire count of 10 at 20 percent bleed yields comparable performance to a wire count of 30 at 5 percent bleed, therefore a substantial savings on bleed air may be realized by tripling the wire count. A further item to note is that current draw becomes larger as wire count is increased because it takes more energy to maintain temperature in a material with larger surface area.

To evaluate the behavior of the control system amidst disturbances not captured by the CES test bed, e.g., impact loads, flight maneuver loads, and sudden changes in altitude, step response tests were conducted on the baseline actuator design (10 wires, 100 percent SOA bleed). To conduct the evaluation, a 0.005-inch change in

TABLE 5.—EFFECT OF COOLING AIR FLOW AND WIRE COUNT
ON CLEARANCE CONTROL PERFORMANCE

Wire Count	Wire Diam. (in)	Control Performance Metrics	Cooling air diverted from Fan as % of SOA peak air flow bleed in ft^3/min in parentheses			
			Baseline 100% (1897)	20% (379)	5% (95)	1% (19)
10	0.092	Min. clearance (mils)	5.0	5.0	1.1	-18.4
		1-mil convergence (sec)	21.8	22.0	35.2	85
		A_f holding current (A)	562	407	322	268
30	0.053	Min. clearance (mils)	5.0	5.0	4.7	1.9
		1-mil convergence (sec)	18.6	21.6	21.5	27.2
		A_f holding current (A)	814	568	433	336

TABLE 6.—STEP RESPONSE SETTLING TIME
AT VARIOUS OPERATING POINTS

CES Operating Point	Martensite Fraction ξ (%)	Settling Time (sec)	
		+0.005 in	−0.005 in
Pinch Point	95.4	3.14	3.19
Climb	37.3	3.03	3.26
Cruise	20.5	3.01	3.27
Descent	0.9	3.03	3.38

clearance was used to excite the system at several operating points throughout the mission. Two opposing steps (step up–step down) of this magnitude were each applied at steady state in order to excite minor hysteresis loops. Table 6 summarizes the results of the test at four operating points, occurring over a wide range of martensite fractions, indicating that the evaluation spans a large portion of the actuator's operable range. Slightly slower response times associated with negative steps are indicative of the fact that the current must saturate at zero upon cooling. Response times are fairly uniform across the operating space, confirming that the effect of nonlinearities and hysteresis is small and that the system is nearly stationary. The narrow hysteresis band of the HTSMA is particularly advantageous in maintaining uniformity because deadband delays are kept small.

VI. Summary and Conclusions

In this paper, an actuation scheme has been established for blade tip clearance control in aircraft engine turbines using a recently-developed high-temperature shape memory alloy. Shape memory alloys are extremely desirable for active control because of their very high energy density characteristics, physical robustness to high-temperature environments, and freedom to be configured as a device that is actuated entirely by energetic airflows. The actuator concept design utilizes a parallel set of HTSMA wires preloaded in tension by a biasing spring. Elongation of the wires causes the shroud to move away from the blades, providing a failsafe mechanism that avoids blade incursions. A design consisting of 10 wires that are two inches in length was found to satisfy operational requirements at all key operating points in the flight envelope while also satisfying material cycle fatigue and actuator spatial constraint requirements. In an effort to minimize the actuator's package size, ground idle was not accommodated in the design, which is not likely to impact the benefits of this clearance control system.

For the prototype system, wire temperature will be modulated using active resistive heating and passively cooled using convection air diverted from the engine's fan, but it is envisaged that future designs will use heated secondary air to modulate the HTSMA to avoid costly modifications to on-board power systems. Cooling is of primary concern for the present actuator because the actuator must retract at roughly 0.01 in/sec during the takeoff transient so that a 0.005-inch clearance can be maintained without causing blade rubs.

Using a detailed model of the actuator coupled with a candidate aircraft engine simulation, transient simulations show that 10 wires of 0.092-inch diameter are adequate for meeting the rate requirements using a PID control law with anti-windup protection given fan air bleeds comparable to state-of-the-art. Trades between wire count and fan air diversion have also been identified, indicating that substantially lower fan air bleeds are possible by tripling the wire count. The control system performance was shown to be uniform across the range of operating conditions, a favorable result indicating that the controller is relatively insensitive to nonlinearities and hysteresis.

As a result of this study, the present HTSMA actuator concept has been identified as having enormous potential for aircraft engine turbine clearance control. Evaluation of the HTSMA actuator on the NASA tip clearance test rig is warranted in order to mature the present actuator concept.

References

1. Melcher, K.M., Kypuros, J.A., "Toward a fast-response active turbine tip clearance control," *Proceedings of the International Symposium on Air Breathing Engines*, ISABE 2003–1102, 2003.
2. Wiseman, M.W., Guo, T., "An investigation of life extending control technologies for gas turbine engines," *Proceedings of American Control Conference*, vol. 5, 2001, pp. 3706–3707.
3. Geisheimer, J.L., Billington, S.A., Burgess, D.W., "A microwave blade tip clearance sensor for active clearance control applications," *Proceedings of the 40th Joint Propulsion Conference and Exhibit*, AIAA–2004–3720, 2004.
4. Lattime, S.B. and Steinetz, B.M., "Test rig for evaluating active turbine tip clearance control concepts," *Proceedings of the 39th Joint Propulsion Conference and Exhibit*, AIAA–2003–4700, 2003.
5. Chopra, I., "Review of state of art of smart structures and integrated systems," *AIAA Journal*, vol. 40, no. 11, 2003, pp. 2145–2187.
6. Saadat, S., Salichs, J., Noori, M., Hou, Z., Davoodi, H., Baron, I., Suzuki, Y., and Masuda, A., "An overview of vibration and seismic applications of NiTi shape memory alloy," *J. Smart Materials and Structures*, vol. 11, April 2002.
7. Elahinia, M.H. and Ashrafiuon, H., "Nonlinear control of a shape memory alloy actuated manipulator," *J. Vibration and Acoustics*, vol. 124, 2002, pp. 566–575.
8. Portloch, L.E., Schetky, L.M., Steinetz, B.M., "Shape memory alloy adaptive control of gas turbine engine blade tip clearance," *Proceedings of the 32nd Joint Propulsion Conference and Exhibit*, AIAA–96–2805, 1996.

9. Singh, K., Sirohi, J., Chopra, I., "An improved shape memory alloy actuator for rotor blade tracking," *J. Intelligent Material Systems and Structures*, vol. 14, 2003, pp. 767–786.
10. Lockyer, A.J., Martin, C.A., Lindner, D.K., Walia, P.S., Carpenter, B.F., "Power systems and requirements for integration of smart structures into aircraft," *J. Intelligent Material Systems and Structures*, vol. 15, 2004, pp. 305–315.
11. Majima, S., Kodama, K., Hasegawa, T., "Modeling of shape memory alloy actuator and tracking control system with the model," *IEEE Transactions on Control Systems Technology*, vol. 9, no. 1, 2001, pp. 54–59.
12. DeCastro, J.A. and Melcher, K.J., "A study on the requirements for fast active turbine tip clearance control systems," *Proceedings of the 40th Joint Propulsion Conference and Exhibit*, AIAA–2004–4176, 2004.
13. DeCastro, J.A., Melcher, K.J., Noebe, R.D., Gaydosh, D., "Development of a numerical model for high-temperature shape memory alloys," (to be published).
14. Hughes, D. and Wen, J.T., "Preisach modeling of piezoceramic and shape memory alloy hysteresis," *J. Smart Materials and Structures*, vol. 6, 1997, pp. 287–300.
15. Brinson, L.C., "One dimensional constitutive behavior of shape memory alloys: thermomechanical derivation with non-constant material functions and redefined martensite internal variables," *J. Intelligent Material Systems and Structures*, vol. 4, 1993, pp. 229–242.
16. Prahlad, H. and Chopra, I., "Comparative evaluation of shape memory alloy constitutive models with experimental data," *J. Intelligent Material Systems and Structures*, vol. 12, 2001, pp. 383–395.
17. Liang, C. and Rogers, C.A., "One-dimensional thermomechanical constitutive relations for shape memory material," *J. Intelligent Materials and Structures*, vol. 1, April 1990.
18. Incropera, F. and DeWitt, D., *Fundamentals of Heat and Mass Transfer*, John Wiley & Sons, New York, NY, 1996.
19. Visioli, A., "Modified anti-windup scheme for PID controllers," *Control Theory and Applications*, vol. 150, no. 3, 2000, pp. 321–329.
20. Ogata, K., *Modern Control Engineering*, 3rd Edition, Prentice-Hall, Englewood Cliffs, NJ, 1997.

REPORT DOCUMENTATION PAGE

Form Approved
OMB No. 0704-0188

1. AGENCY USE ONLY (*Leave blank*)	2. REPORT DATE	3. REPORT TYPE AND DATES COVERED
	July 2005	Technical Memorandum

4. TITLE AND SUBTITLE

System-Level Design of a Shape Memory Alloy Actuator for Active Clearance Control in the High-Pressure Turbine

5. FUNDING NUMBERS

WBS–22–714–70–42

6. AUTHOR(S)

Jonathan A. DeCastro, Kevin J. Melcher, and Ronald D. Noebe

7. PERFORMING ORGANIZATION NAME(S) AND ADDRESS(ES)

National Aeronautics and Space Administration
John H. Glenn Research Center at Lewis Field
Cleveland, Ohio 44135–3191

8. PERFORMING ORGANIZATION REPORT NUMBER

E–15204

9. SPONSORING/MONITORING AGENCY NAME(S) AND ADDRESS(ES)

National Aeronautics and Space Administration
Washington, DC 20546–0001

10. SPONSORING/MONITORING AGENCY REPORT NUMBER

NASA TM—2005–213834
AIAA–2005–3988

11. SUPPLEMENTARY NOTES

Prepared for the 41st Joint Propulsion Conference and Exhibit cosponsored by the AIAA, ASME, SAE, and ASEE, Tucson, Arizona, July 10–13, 2005. Jonathan A. DeCastro, QSS Group, Inc., 21000 Brookpark Road, Cleveland, Ohio 44135; and Kevin J. Melcher and Ronald D. Noebe, NASA Glenn Research Center. Responsible person, Jonathan A. DeCastro, organization code RIC, 216–433–3946.

12a. DISTRIBUTION/AVAILABILITY STATEMENT

Unclassified - Unlimited
Subject Category: 07

Available electronically at http://gltrs.grc.nasa.gov

This publication is available from the NASA Center for AeroSpace Information, 301–621–0390.

12b. DISTRIBUTION CODE

13. ABSTRACT ***(Maximum 200 words)***

This paper describes results of a numerical analysis evaluating the feasibility of high-temperature shape memory alloys (HTSMA) for active clearance control actuation in the high-pressure turbine section of a modern turbofan engine. The prototype actuator concept considered here consists of parallel HTSMA wires attached to the shroud that is located on the exterior of the turbine case. A transient model of an HTSMA actuator was used to evaluate active clearance control at various operating points in a test bed aircraft engine simulation. For the engine under consideration, each actuator must be designed to counteract loads from 380 to 2000 lbf and displace at least 0.033 inches. Design results show that an actuator comprised of 10 wires 2 inches in length is adequate for control at critical engine operating points and still exhibits acceptable failsafe operability and cycle life. A proportional-integral-derivative (PID) controller with integrator windup protection was implemented to control clearance amidst engine transients during a normal mission. Simulation results show that the control system exhibits minimal variability in clearance control performance across the operating envelope. The final actuator design is sufficiently small to fit within the limited space outside the high-pressure turbine case and is shown to consume only small amounts of bleed air to adequately regulate temperature.

14. SUBJECT TERMS	15. NUMBER OF PAGES
Clearances; Turbines	20
	16. PRICE CODE

17. SECURITY CLASSIFICATION OF REPORT	18. SECURITY CLASSIFICATION OF THIS PAGE	19. SECURITY CLASSIFICATION OF ABSTRACT	20. LIMITATION OF ABSTRACT
Unclassified	Unclassified	Unclassified	